Atmospheric Environment: X 2 (2019) 100012

Contents lists available at ScienceDirect

Atmospheric Environment: X

journal homepage: www.journals.elsevier.com/atmospheric-environment-x

Spatially dense air pollutant sampling: Implications of spatial variability on the representativeness of stationary air pollutant monitors

Hugh Z. Li[a], Peishi Gu[a], Qing Ye[a], Naomi Zimmerman[a,1], Ellis S. Robinson[a], R. Subramanian[a], Joshua S. Apte[b], Allen L. Robinson[a], Albert A. Presto[a,*]

[a] Center for Atmospheric Particle Studies, Carnegie Mellon University, Pittsburgh, PA, 15213, United States
[b] Department of Civil, Architectural and Environmental Engineering, The University of Texas at Austin, Austin, TX, 78712, United States

HIGHLIGHTS

- Air pollutant spatial variations are a function of pollutant and land use.
- Mobile monitoring shows that urban stationary monitors represent areas < 1 km^2.
- Variation in pollutant concentration is related to spatial variability in land use.

GRAPHICAL ABSTRACT

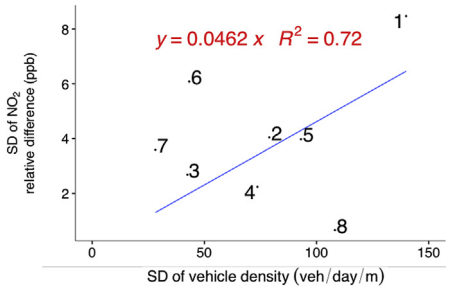

ARTICLE INFO

Keywords:
Particulate matter
Exposure
Low-cost sensors
Spatial variations

ABSTRACT

Long- and short-term exposure to airborne pollutants results in adverse health effects. Regulatory monitors can be used to determine if regional concentrations meet regulatory standards of air pollution. As assessments of air pollutant exposure become more spatially resolved, evaluation is needed to assess the spatial representativeness of monitors in different environments. We measured NO_2, ultrafine particle concentration (UFP), and PM_1 with both stationary and mobile platforms in Pittsburgh, PA in 2016 and 2017. We sampled in eight ~1 km^2 neighborhoods representing different land use and exposure regimes (e.g., urban and suburban, high and low traffic). Mobile sampling was conducted on up to 25 days in each neighborhood to study fine-scale spatial variation in pollutant concentrations. NO_2 exhibited within-neighborhood spatial variation, with hotspots elevated by up to a factor of 5 above the regional background. Spatial differences in UFP within the same 1 km^2 neighborhoods could be a factor of 2.4 times regional background. PM_1 was more regional and less spatially variable. Most neighborhoods exhibited less than 1 μg m^{-3} spatial variability in PM_1. Spatial variability of NO_2 and UFP showed moderate correlation ($R^2 > 0.5$) with traditional land use covariates such as traffic volume and restaurant density. We used the Wilcoxon rank-sum test to calculate the fraction of each neighborhood represented by the same underlying concentration distribution. PM_1 was the most spatially homogeneous, with 80–100% of each 1 km^2 area being statistically similar to a reference location. Quantifying pollutant spatial patterns with high fidelity (e.g., < 2 ppb NO_2 or < 1 μg m^{-3} PM_1) seems unattainable in many urban areas unless the sampling network is significantly dense, with more than one or two nodes per km^2.

* Corresponding author.
E-mail address: apresto@andrew.cmu.edu (A.A. Presto).
[1] Current address: Department of Mechanical Engineering, University of British Columbia, British Columbia, Canada.

https://doi.org/10.1016/j.aeaoa.2019.100012
Received 18 July 2018; Received in revised form 9 November 2018; Accepted 22 January 2019
Available online 31 January 2019

1. Introduction

Air pollution exposure is associated with numerous adverse health effects, including cardiovascular disease, diabetes, and lung cancer (Brook et al., 2010; Cohen et al., 2017; Di et al., 2017a, 2017b; Lim et al., 2012; Pope et al., 2009; Raaschou-Nielsen et al., 2013; Strak et al., 2017). Long-term exposure to fine particulate matter ($PM_{2.5}$) is accountable for 7 million premature deaths annually (Brauer et al., 2016). Even in areas that meet the U.S. Environmental Protection Agency (EPA) air quality standards, chronic exposure to $PM_{2.5}$ contributes to excess health risks (Di et al., 2017b). The PM dose-response curve is super linear at low concentrations (Burnett et al., 2014; Di et al., 2017a, 2017b) so concentration reductions beyond the current EPA and World Health Organization air quality standards continue to accrue benefits (Marshall et al., 2015). Short-term exposures to $PM_{2.5}$ are also relevant. Di et al. (2017a) recently demonstrated that a $10\,\mu g\,m^{-3}$ increase of daily (24-hr) $PM_{2.5}$ exposure was significantly associated with a relative increase of 1.05% in mortality rate, even at concentrations below national air quality standards.

While $PM_{2.5}$ exposure dominates the health risks and costs associated with air pollution exposure (Cohen et al., 2017), other air pollutants can impact human health. The EPA regulates seven criteria pollutants ($PM_{2.5}$, PM_{10}, CO, NO_2, O_3, SO_2, Pb) through ambient concentration standards. In addition to these pollutants, particle number (PN) concentration, especially the concentration of ultrafine particles (UFP, particles with diameter less than 100 nm), is a pollutant of concern because it may have health effects distinct from $PM_{2.5}$ mass (Hama et al., 2017; Health Effects Institute, 2013; Kerckhoffs et al., 2016; Klompmaker et al., 2015; Leoni et al., 2016). UFP is highly dynamic in both space and time (Klems et al., 2010). Due to its small physical size, UFP can penetrate deep into the respiratory system, thus potentially causing a more direct impact on human health (Stafoggia et al., 2017).

Regulatory monitoring networks, such as the EPA Air Quality System (AQS), are essential tools for monitoring compliance with ambient air pollution standards. They are also a valuable resource for evaluating predictions from chemical transport models (CTMs) (Friberg et al., 2017). However, regulatory-grade instruments at individual monitoring stations are expensive and costly to maintain, and therefore stations are sparsely distributed. Numerous studies have shown that both individual pollutant concentrations (Eeftens et al., 2012; Li et al., 2016; Wang et al., 2013) and $PM_{2.5}$ composition (Li et al., 2018; Tan et al., 2016, 2014a) have small-scale spatial variations that are not captured by the regulatory network. These spatial variations create variations in human pollutant exposures and resultant health impacts (Di et al., 2017b; Jerrett et al., 2005).

Multiple lines of research have emerged with the goal of better characterizing spatial variations in air pollutant concentrations, including low-cost sensor networks, mobile sampling, and improving the spatial resolution of CTMs to $\sim 1\,km^2$. Increased availability of low-cost sensors has fostered interest in deploying them for ambient applications (Kumar et al., 2015; Snyder et al., 2013; Zimmerman et al., 2018a). One primary application of these sensor networks is to supplement regulatory monitors and provide spatially-resolved air pollutant concentration fields. These lower-cost sensor networks hold promise to inform pollutant spatial patterns, and therefore gradients in human exposure, with high fidelity due to advances in calibration algorithms and sensor quality (Cross et al., 2017; Jiao et al., 2016; Spinelle et al., 2015; Zimmerman et al., 2018a).

One important and often unanswered question relevant to the deployment of both regulatory monitors and lower-cost sensors is the spatial representativeness of the monitoring locations. To first order, we expect a monitor in a rural park to be representative of a larger area than a roadside location in an urban street canyon (Piersanti et al., 2015; Vardoulakis et al., 2005). For example, Vitali et al. (2016) determined that an industrial air quality monitoring station was representative of a roughly 250 m by 250 m area, and Shi et al. (2016) used geostatistical methods determine that $PM_{2.5}$ concentrations in Hong Kong varied significantly over spatial scales of 300 m. However, we are unaware of any studies that attempted to characterize the spatial representativeness of multiple stationary pollutant monitors located in different microenvironments across an entire city.

Traditionally, regional CTMs have been operated with spatial resolution on the order of tens of kilometers (e.g., 16×16 or 32×32 km; Roohani et al., 2017). Model skill is evaluated by comparison of simulation results to reference network measurements, typically using monitors located in the urban background or other locations with minimal source impacts (Friberg et al., 2017). Increasing CTM spatial resolution, for example modeling at $1\,km^2$ resolution over a city, introduces two specific challenges. First, a larger number of sampling locations are required to evaluate model performance. Distributed networks of low-cost sensors can be used for this purpose. Second, the variability within each grid cell needs to be known in order to constrain uncertainties. Unless low-cost sensors are deployed at very high spatial densities (> 1 per km^2), they cannot inform the sub-grid-scale variability.

Mobile monitoring is well suited to quantify pollutant spatial variations at fine (sub-km) length scales. Numerous studies have demonstrated the ability of mobile sampling to resolve pollutant spatial differences near specific sources (e.g., roadways), as well as to map neighborhood-level differences within a city (Apte et al., 2017; Deshmukh et al., 2016; Hankey and Marshall, 2015; Li et al., 2018, 2016; Steffens et al., 2017; Ye et al., 2018). A major challenge with mobile sampling is to collect enough data in a given location to accurately quantify annual- or other long-term average concentrations, though identifying hotspots or consistent gradients between neighborhoods requires less data (Tan et al., 2014b; Apte et al., 2017; Messier et al., 2018).

This manuscript combines mobile and stationary sampling to better understand sub-km variability in pollutant concentrations and to quantify the spatial representativeness of pollutant concentrations measured by stationary monitors. We coupled mobile and stationary sampling in a variety of neighborhoods in a single U.S. urban area in order to address three specific questions: (1) How spatially representative is a stationary pollutant monitor? (2) How does the spatial representativeness of a stationary pollutant monitor vary with modifiable factors related to land use and emissions? (3) What impact does spatial representativeness have on the ability of CTMs to predict concentration fields? By extension, our analysis allows us to determine how many monitors are needed per km^2 to quantify pollutant concentrations within specified tolerances as a function of land use and urban form.

2. Material and methods

This study combines mobile and distributed stationary sampling. Data were collected as part of the Center for Air, Climate, and Energy Solutions (CACES) air quality observatory (Zimmerman et al., 2018b). The stationary samplers provide data on the long-term differences in pollutant concentrations between urban neighborhoods (e.g., downtown central business district versus residential versus an urban park). Mobile sampling is layered on top of the network of distributed samplers in order to characterize small-scale (sub-km) variability around each stationary sampler. The combined dataset, therefore, informs average concentrations in specific neighborhoods along with the spatial variation within each neighborhood; these data can then be used to understand how spatially representative each stationary sampling location is as well as to understand the potential uncertainty in model-measurement agreement for CTM evaluation as a function of stationary sensor placement.

Measurements were conducted in Allegheny County, PA, which is centered around the City of Pittsburgh. The county's landscape is characterized by a plateau cut by three river valleys. The air quality is influenced by the interaction of regional pollutants transported from

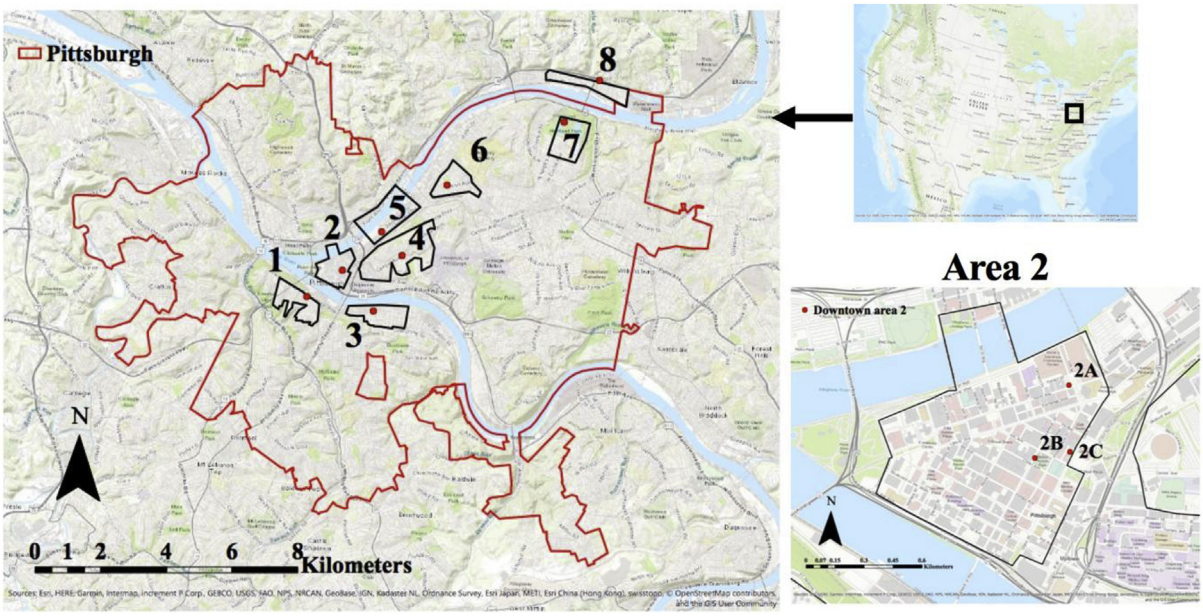

Fig. 1. Overview of the sampling domain in Pittsburgh and Allegheny County, PA. Sampling sites and neighborhoods are numbered according to the predominant wind direction—southwest to northeast. The locations of the stationary monitors are indicated with red circles. Mobile sampling was conducted in ~1 km^2 areas around the stationary monitors, as shown with the black polygons. The mobile sampling areas roughly corresponded to the boundaries of specific neighborhoods. Each neighborhood had one stationary monitoring site with the exception of neighborhood 2, which had three stationary samplers as shown in the bottom right panel.

power plants and other upwind industrial emissions with local industrial and traffic sources. Diverse point sources are distributed in the county, including the largest metallurgical coke plant in the U.S., steel manufacturing facilities, and power plants.

2.1. Sampling campaign overview and neighborhood selection

As noted above, the sampling campaign included a combination of distributed stationary monitors with mobile sampling around each stationary monitor (Fig. 1). Herein, we adopt the following nomenclature. Stationary monitors are referred to as "sites." The corresponding mobile sampling domain around each site is called an "area" or "neighborhood." Table 1 lists all of the sampling sites/areas in this study, as well as the dates of operation for the stationary samplers. There is one stationary sampler per driving area, except area 2, which covers the Pittsburgh downtown central business district and has three monitors.

Fig. 1 and Table 1 show the locations and details of each sampling area. The sites in Table 1 are numbered along the prevailing wind direction. Regional winds are typically from the southwest (Supplemental Information, Fig. S1), so the sampling sites cover an area from upwind of the downtown central business district to downwind residential areas.

The sampling sites were selected to span a variety of micro-environments. All sampling areas were classified with three stratification variables (Table 1) to represent the impacts of local sources and land use on measured pollutant concentrations. These stratification variables are traffic, restaurants, and building height. Traffic (Apte et al., 2017; Karner et al., 2010; Saha et al., 2018a) and restaurants (Robinson et al., 2018; Vert et al., 2016) are chosen because they are associated with known air pollutant emissions sources. We expect higher pollutant concentrations in high-traffic and high-restaurant areas. Building height is selected as a proxy for street canyon effects, which is a land use factor that can modify concentration patterns near roadways (Tang et al., 2013).

Stratification for each of these variables is binary. For example, each area is either 'high traffic' or 'low traffic' as shown in Table 1. Table 1 lists the mean value of each stratification variable for each area, as well as the overall classification of that area as 'high' or 'low' for that variable. The traffic criterion is vehicle density determined from annual average daily traffic counts (AADT) divided by road length (vehicles per day per meter). The restaurant criterion is restaurant counts per square km. The building height criterion is the mean building height in the neighborhood. Data for land use stratification are collected from several

Table 1
Overview of the sampling network. Site/Area ID is defined based on geographic locations from southwest to northeast, consistent with prevailing wind direction. Sites/areas are classified as either high (H) or low (L) for each of three stratification variables. The mean value for each stratification variable in each area is reported.

Area ID	Site name	Traffic (Veh/day/m)	Restaurant (km^{-2})	Building height (m)	Distributed monitor operating dates	Number of mobile sampling days
1	Mt Washington	2.4 (L)	14 (L)	3 (L)	01/2017–03/2017	10 (Winter 10)
2	Downtown-Penn (2A) Downtown-Mellon (2B) Downtown-Grant (2C)	15.8 (H)	141 (H)	49 (H)	01/2017–03/2017	25 (Summer 6, Winter 19)
3	South Side	3.7 (H)	71 (H)	8 (H)	01/2017–03/2017	16 (Summer 2, Winter 14)
4	Hill District	3.3 (H)	9.4 (L)	7 (H)	08/2016–03/2017	19 (Summer 8, Winter 11)
5	Strip District	5.1 (H)	25 (H)	17 (H)	08/2016–09/2016	18 (Summer 11, Winter 7)
6	Lawrenceville	4.2 (H)	47 (H)	8 (H)	08/2016–03/2017	14 (Summer 11, Winter 3)
7	Highland Park	2.3 (L)	5.5 (L)	3 (L)	08/2016–09/2016	12 (Summer 7, Winter 5)
8	Aspinwall	6.4 (H)	11 (L)	3 (L)	08/2016–09/2016	9 (Summer 6, Winter 3)

publicly-available sources (Allegheny County Information Portal, 2017; Department of City Planning, 2017; City of Pittsburgh GIS Data, 2015; US Census Tiger, 2010).

Mobile sampling was conducted inside a predetermined ~1 km^2 area around each stationary monitor, shown by the black polygons in Fig. 1. We tried to center the stationary monitors within each driving area, as this would help us answer if the monitor would be representative of its surrounding air pollution pattern, though this was not possible for every neighborhood. The 1 km^2 neighborhoods were selected to represent different land uses, and the boundaries of the sampled neighborhoods generally match with the boundaries of neighborhoods as defined by the city of Pittsburgh. For example, neighborhood 2 coincides with the downtown central business district and is 'high' in all three stratification variables. Neighborhoods 3 (South Side) and 6 (Lawrenceville) are mixed-use commercial and residential areas; while they are 'high' in all three stratification variables, they have less traffic, fewer restaurants, and shorter buildings than downtown. Purely residential areas like neighborhood 1 (Mt. Washington) and 7 (Highland Park) are 'low' for all three stratification variables.

Mobile sampling was conducted on weekdays during dry conditions to avoid biases due to weekday-weekend emissions patterns and from pollutant rainout. Each time we sampled in a neighborhood, we drove through all public roads at least once. Sampling typically took 45–60 min per neighborhood, and we typically sampled 3–5 neighborhoods on each sampling day. For each neighborhood, measurements were taken during morning (5–10 AM), midday (11 AM-4 PM) and evening (5–10 PM) periods on different days, so that concentration data are not biased due to the time-of-day patterns of local emissions. Each area was visited on at least nine different weekdays spread in summer (August and September) and winter (November–February). Details of the mobile sampling are shown in Table 1, and additional information on the mobile sampling strategy is described in Gu et al. (2018) and Zimmerman et al. (2018b).

2.2. Air pollutant measurements

The sampling network was composed of a mobile laboratory and distributed stationary monitors. Table S1 in the Supplemental Information outlines the full suite of instruments as well as the sampling and calibration frequencies. The distributed monitors were all equipped with a low-cost sensor package, the real-time affordable multipollutant sensor (RAMP), to measure concentrations of gaseous pollutants. The RAMP was described in detail in Zimmerman et al. (2018a) and Malings et al. (2018). Briefly, the core components of the RAMP were Alphasense electrochemical sensors (Alphasense Ltd., UK) for measuring CO, O_3, SO_2, and NO_2. Raw sensor outputs were converted to concentrations using a previously developed machine learning calibration (Zimmerman et al., 2018a). The RAMPs reported gas concentrations every 15 s, which were further down averaged to 15 min for data management purposes.

The distributed monitors were also equipped with MetOne Neighborhood PM monitors (MetOne Instruments, Inc., OR, USA) to quantify optical $PM_{2.5}$ mass via nephelometry. We applied a humidity-based hygroscopic growth factor correction (Petters and Kreidenweis, 2007) to reduce errors due to particle-bound water at high relative humidity. Some of the distributed monitors had a co-located water-based condensation particle counter (Aerosol Dynamics Inc., Berkeley, CA) for quantifying particle number (PN) concentration, which we use as a proxy for UFP concentrations. $PM_{2.5}$ and UFP measurements were reported along with gaseous pollutants at 15 s resolution and down averaged to 15-min resolution.

A mobile laboratory was used to examine pollutant spatial patterns around each stationary monitor. The mobile laboratory was a gasoline-powered van that has been described in detail previously (Li et al., 2016; Tan et al., 2014a). Power was drawn from the van engine via a converter and then dispatched to instruments. Two stainless steel sampling lines were installed on top of the van. The sampling inlets were about 4 m above the ground and located in front of the vehicle exhaust to avoid self-sampling. A Bad Elf GPS logger (Bad Elf, CT, USA) recorded the mobile sampling location every 1 s.

While we did not specifically test for impacts of self-sampling in this study, we have considered it extensively in the past and found it to be negligible (Tan et al., 2014a; Li et al., 2016; Robinson et al., 2018). In order for self-pollution to be a major concern under most driving conditions, the wind needs to be coming from the tail of the vehicle at a speed faster than our typical driving speed (~20–25 miles per hour). Tan et al. (2014a) found that the incidence of pure tail winds was a small fraction of the sampling time (mean = 7%), and Robinson et al. (2018) saw no evidence of self-sampling in aerosol mass spectrometer data collected while in motion.

The mobile laboratory uses two sample inlets. One sampling line was for particle measurements including PM_1 (particulate matter < 1 μm diameter) composition measured by a Time of Flight Aerosol Mass Spectrometer (AMS) (Aerodyne Research Inc., Boston, MA) (DeCarlo et al., 2006; Jayne et al., 2000), black carbon (BC) by Aethalometer (Magee Scientific AE-33, CA, USA), and ultrafine particle number (UFP) from a Fast Mobility Particle Sizer (FMPS, size range 5.6–560 nm) (TSI Incorporated, MN, USA). We did not design the sampling probe to be isokinetic under in-motion sampling conditions. Before the air flow reached these particle instruments, it was size selected with a 2.5 μm cyclone at a controlled flow of 16.7 SLPM. The sum of particle composition from the AMS (organic and inorganic) plus the BC from Aethalometer yielded the PM_1 mass. The AMS was operated in fast mass spectrum mode and output data at 20 s resolution (Kimmel et al., 2011). BC data were recorded at 1-min resolution.

The FMPS raw output was calibrated based on Zimmerman et al. (2015). The FMPS is prone to vibrational interference that can create unrealistic size distributions during mobile sampling. Fig. S2 (Supplemental Information) shows an example of an FMPS size distribution impacted by vibrational interference. The ~40–60 nm size bins reported zero particle counts when the van hit a bump on the road, creating unrealistic size distributions. FMPS data were therefore filtered based on the number of zeros in middle size bins during analysis to remove these instances. UFP concentrations were reported every 1 s.

The other sampling line was for gas phase instruments, including a NOx analyzer (API-Teledyne T200) and CO analyzer (API-Teledyne T300). A HEPA filter was placed in the sampling line to remove particles before sample air reached the gas instruments. All gas instruments reported data every 1 s.

2.3. Data treatment and QA/QC

Routine calibration and maintenance were performed for both sampling platforms. Table S1 in the Supplemental Information lists the frequency of calibrations for all instruments in the mobile lab and the stationary monitors. All gas monitors used in the mobile laboratory were calibrated weekly, and all calibrations were zero/span checks. We did not perform multi-point calibrations for gas monitors.

An AMS ionization efficiency calibration was performed every time the AMS was unloaded and reloaded from the mobile laboratory. The AMS collected one HEPA filtered blank sample per day for use in air beam corrections. The FMPS was zero cleaned by attaching a HEPA filter at the inlet and observing the fall in particle counts. This was done before each sampling trip.

The gas sensors used in the distributed monitors were calibrated according to the method outlined by Zimmerman et al. (2018a) via co-location with reference monitors prior to deployment in the field. After deployment (deployment periods are listed in Table 1), the calibration was checked again via co-location with reference monitors. As reported by Zimmerman et al. (2018a) and Malings et al. (2018), we observed minimal drift in the pre- and post-calibration and therefore no post-

corrections were made to the data.

The MetOne $PM_{2.5}$ output was first corrected based on hygroscopic growth factor (Petters and Kreidenweis, 2007), and then further corrected using a linear regression against reference PM monitors (BAM-1020, MetOne Instruments, Inc., OR, USA) at a nearby regulatory monitoring station (Malings et al., in prep).

The raw output from the distributed CPCs was adjusted based on co-location tests with a butanol CPC (TSI Incorporated, MN, USA) in the lab (Saha et al., 2019). We eliminated any CPC data with error codes, counts less than 100 cm^{-3} (an indication of a dry wick) or counts greater than 1,000,000 cm^{-3} (spikes due to power cycling).

Stationary monitor measurements were filtered for extreme concentrations. Outlier filtering followed the method used in the ESCAPE study; outliers are defined as values either larger than the 75th percentile plus four times the interquartile range or less than the 25th percentile minus four times the interquartile range (de Hoogh et al., 2013). This outlier filtering only applied to distributed monitor data. Mobile sampling data were expected to show more episodic events and broader concentration range compared with stationary monitor measurements because of spatial source impacts and different resolution in instrumentation (Tan et al., 2014a), so the mobile data were not filtered.

We took additional QA/QC steps to ensure that mobile sampling data were not driven by error or non-representative spikes. Each sampling drive had a co-pilot whose main task was to log spike events and identify doubtful peaks (e.g., a large spike in CO or NO_2 in a park with no vehicles nearby). When we analyzed the raw data, we referred to these notes to screen out low-quality data, though these sorts of spikes are exceedingly rare.

Mobile measurements of 1 Hz gases and UFP were spatially allocated to 50 m grid cells based on GPS information after correcting for residence time in the sampling line. PM_1 was reported at 20 s resolution. Therefore, we employed 100 m grid cells and joined PM_1 measurements to the mean GPS latitude and longitude in each 20-s time window.

2.3.1. Temporal corrections

Mobile sampling convolves temporal and spatial variations in measured concentrations. Isolating the spatial variations, therefore, requires background subtraction to remove temporal fluctuations due to, for instance, boundary layer shifts over the course of the day. We applied two temporal corrections to the mobile data used here; the methods are described briefly below and shown in detail in the Supplemental Information.

The first correction method is a variation of the rolling constant percentile subtraction method applied in other studies (Brandt, 2007; Larson et al., 2017; Simon et al., 2017; Gu et al., 2018). We first smooth the high frequency (1-Hz or 20-sec) data with a 1-min median to remove short-term spikes caused by nearby sources. We then calculate the 5th percentile of the smoothed data in a rolling 1-h window. We define this 5th percentile as the temporally-varying regional background; concentrations in excess are deemed local variations. The time base of one hour was selected because a visit to each 1 km^2 neighborhood took about one hour. We typically drove in regional background areas during transit between neighborhoods. Thus, within each one-hour period there is data collected in a regional background location. Fig. S3 in the SI shows the sensitivity of the background correction to the averaging time window. Using a time base of thirty minutes or two hours did not result in statistically different background concentrations.

A second background correction leverages the stationary sampling monitors. We first use wavelet decomposition (Klems et al., 2010; Sabaliauskas et al., 2014) to isolate concentration changes occurring with time variation greater than 8 h at each stationary sampling monitor. Then, for each 15-min sampling window, we define the monitor with the minimum decoupled concentration as the regional background and subtract this value from the mobile sampling data.

The two background correction methods are compared in Fig. S4. For the times of day containing the majority of mobile sampling data (~6 am–9 pm), the two methods agree within ~2 ppb for NO_2 and < 1 μg m^{-3} for PM_1. We chose the wavelet correction method for NO_2 and PM_1 because stationary monitors are less affected by local source impacts and their continuous operation provides a more accurate description of temporal variation (Brantley et al., 2014). We apply the rolling 5th percentile corrections for UFP because not every site had a CPC, and because of extensive downtime for some of the CPCs during concurrent mobile sampling periods.

2.3.2. Representativeness of mobile sampling data

In addition to temporal corrections described above, the second challenge with mobile sampling is the limited number of data points collected at each spatially distributed location. Even after temporal correction, mobile sampling data within a specific grid cell must be summarized over a sufficient number of data points (or days) to obtain a concentration, and concentration pattern, that is representative of long-term conditions.

Several studies have investigated data requirements for mobile and distributed sampling (Apte et al., 2017; Hatzopoulou et al., 2017; Tan et al., 2014b), though a specific consensus on data requirements for mobile sampling has not been agreed upon in the literature. One recent paper by Apte et al. (2017) oversampled a small area of Oakland, CA and conducted mobile sampling on 50 unique days. Systematic subsampling of this massive dataset showed rapid improvement in both correlations with the long-term median and reduction in error up to 10 sampling days, modest improvement from 10 to 20 days, and less improvement for 20–50 days. To first order, this suggests that between 10 and 20 sampling days per grid cell are required to determine robust long-term (annual or seasonal) concentrations, though data requirements for determining spatial patterns (e.g., ranking each grid cell or identifying hot spots) is smaller (Tan et al., 2014b; Van den Bossche et al., 2016).

We tested the mobile sampling requirements for our dataset using the stationary samplers. Fig. S5 in the Supplemental Information shows the result of bootstrap resampling of data collected at two stationary monitors: 2A and 4. For this analysis, we randomly selected a single data point from each of *N* days, where *N* ranged from 1 to 50. This selection was iterated 1000 times for each value of *N* in order to determine the bootstrapped median concentration. For each of the pollutants of interest (PM_1, NO_2, and UFP), the subsampled median converges to the actual median after 5-10 separate sampling days. Additional samples after the 10th day reduce the uncertainty in the subsampled median. Thus, our stationary data seem to verify that approximately ten days of mobile sampling are required to resolve robust spatial patterns. Alternatively, the bootstrap resampling can be conducted for a specific number of data points collected in a single grid cell, regardless of whether or not some are collected on the same day. Our analysis shows that a stable median is reached after ~20 samples per 50 m grid cell.

3. Results and discussion

3.1. Agreement between mobile vs. distributed monitors

The first step in our analysis is to compare the mobile and stationary measurements. While we do not expect perfect agreement between the two sampling platforms (e.g., mobile and stationary sampling locations are not identical), we do expect to observe a similar spatial pattern. Fig. 2 shows the comparison of mobile and stationary measurements of NO_2. Overall, the two platforms agree for NO_2, and we observed similar agreement for the other measured pollutants. Concurrent NO_2 measurements from mobile sampling and distributed monitors showed moderate correlation (Pearson's r, 0.51). Both the mobile and stationary datasets describe a similar NO_2 urban enhancement, with ~5 ppb more

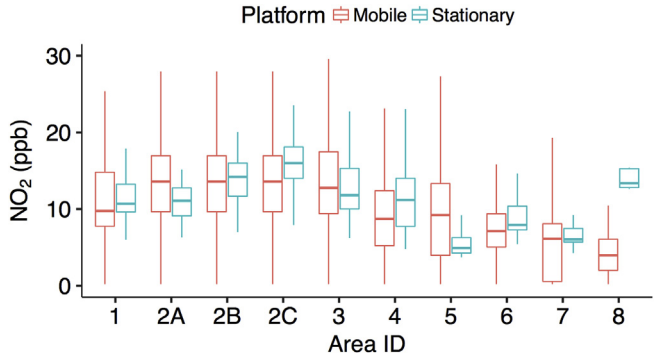

Fig. 2. Contemporaneous NO_2 measurement comparison between distributed monitors and mobile measurements inside corresponding 1 km^2 areas. The top and the bottom of the boxes represent the 75th and 25th percentiles. The line inside the box is the median. The whiskers extend to the most extreme concentrations not classified as outliers.

NO_2 for urban areas 2 and 3 compared to downwind area 7. The mobile data are more variable than the stationary data (e.g., larger interquartile range), as would be expected for on-road sampling.

Downwind area 8 exhibited the largest discrepancy between mobile and distributed monitor. This occurred because the stationary sampler was located ~5 m from a highway, whereas the nearest road sampled by the mobile laboratory was ~50 m from the stationary sampler. The roads sampled in area 8 were also generally upwind of the stationary sampler. Thus, the stationary monitor measured higher concentrations of NO_2 than mobile measurements. This illustrates the rapid decay of traffic-related pollutants within 100–200 m away from roads (Karner et al., 2010).

3.2. Mobile sampling: spatial variability in each area

Mobile sampling shows that, as expected, pollutant concentrations are spatially variable within each area. Fig. 3 shows the temporally-corrected NO_2 variability mapped at 50 m spatial resolution inside each mobile sampling area. Each sampling area is similar in total size (~1 km^2), but the number of sampled 50-m grid cells in each area varies based on road density. Urban areas, therefore, have larger numbers of 50-m grid cells than suburban areas.

The color of each grid cell in Fig. 3 represents the NO_2 enhancement, which is the median NO_2 concentration above the regional background. Grey cells are within 50% of the regional background (7 ppb in the study region), with values ranging from 4 to 10 ppb. Yellow cells have median concentrations that are double the background, and red cells are three times higher than the background. Grid cells without a color fill are ones with insufficient data, as defined above in section 2.3.2. For this analysis, we only consider grid cells with at least 20 mobile data points over 9 or more sampling days.

As expected, we observe both intra- and inter-area variability in NO_2 concentrations. Area 1, which is largely residential and low traffic, is essentially background with little or no NO_2 enhancement. Area 2, which includes the downtown central business district, has both the largest absolute NO_2 enhancement above the regional background as well as significant inter-grid variability, with concentrations ranging from background to 51 ppb. This is due to the combined influence of traffic and building height induced street canyon effects (Harrison, 2018). Area 3, another urban sampling area, is less spatially variable than area 2 but is consistently elevated above the background. Areas 4, 5 and 6, which have a mixture of residential and commercial areas, have more than half of their 50 m grid cells as grey regional background. One grid cell in area 6 located at the junction of several major streets has the highest NO_2 enhancement across all the neighborhoods. Downwind areas 7 and 8 have both lower concentrations and less spatial variability and resemble area 1.

Fig. 3 shows that there is different NO_2 spatial variability in various neighborhoods. Urban areas tend to have both higher NO_2 concentrations and sizeable spatial heterogeneity (average interquartile range, IQR, of NO_2 enhancement for areas 2–6 is 3 ppb) than background suburbs (average IQR of NO_2 enhancement for areas 1, 7, and 8 is 1 ppb), which means that a reference monitor located in an urban center might be less representative of nearby concentration fields. This finding also suggests greater uncertainty in CTM predictions when

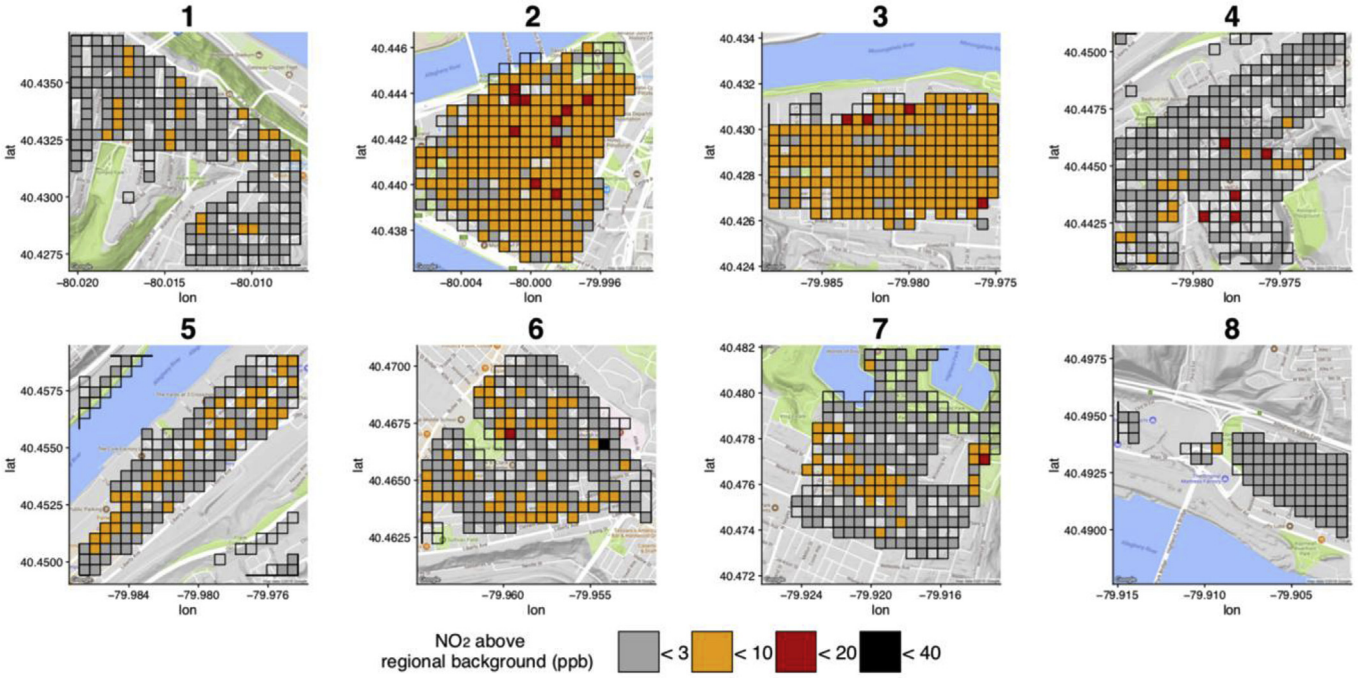

Fig. 3. Temporally corrected median NO_2 enhancement above regional background across all sampling days mapped with 50 m resolution inside eight ~1 km^2 mobile driving areas. Area number is labeled on top with details listed in Table 1.

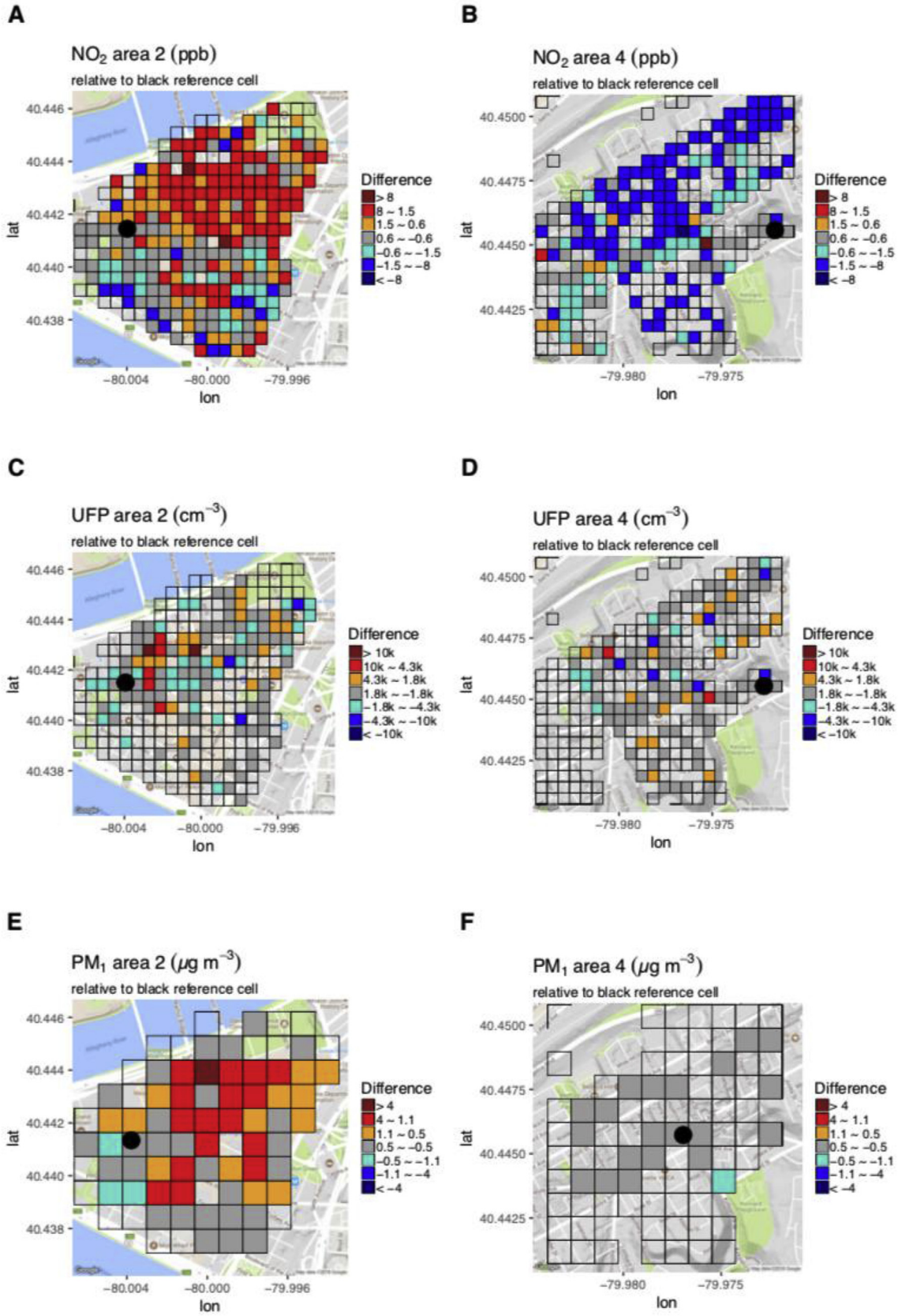

Fig. 4. Spatial variation of (A–B) NO_2, (C–D) UFP, and (E–F) PM_1 relative to pseudo monitor in the 1 km^2 mobile driving areas 2 and 4. Grid cells are colored based on the median concentration difference relative to the reference cell (black dot). The PM_1 maps have larger grid cell size (100 m vs. 50 m) due to the lower temporal resolution of the measurements.

comparing to urban monitors than rural or remote regulatory monitors. CTMs divide the prediction area into grid cells and assume that point measurements from a monitor can represent the entire grid cell (Friberg et al., 2017). Fig. 3 suggests that concentration patterns in 1 km^2 CTM grids may not have a single representative concentration.

3.3. Spatial concentration differences relative to pseudo monitors

In this section, we use the temporal variations measured by the distributed monitors (Fig. S6, Supplemental Information) to assist in mapping 'true' spatial variations relative to pseudo monitors. Results for the central business district (area 2) and an urban residential neighborhood (Hill District, area 4) are shown in Fig. 4. Additional comparisons are shown for area 6 and 7 in Fig. S7 (Supplemental Information). We define a reference cell for each area, indicated by a black dot. The reference cell has data collected on each mobile sampling day and the most total data points in each area and is therefore chosen as the most representative cell in each neighborhood.

Fig. 4 compares spatial concentration differences between cells to the typical hour-to-hour temporal differences measured by the stationary monitors. Fig. S6 shows cumulative distribution functions (CDFs) of hourly pollutant concentration differences (e.g., 4 pm minus 3 pm). For each pollutant, both the mode and the median hour-to-hour difference is zero. Within a given day, hour-to-hour changes in concentrations measured at stationary monitors tend to be small. This is reflected in typical diurnal patterns that show modest changes in consecutive hours (de Foy, 2018).

Fig. 4 uses the 50% cut-points of temporal variation (red lines in Fig. S6) to evaluate spatial variations. Spatial variations larger than the 50% range of hourly temporal variations are deemed significant, whereas spatial variations smaller than typical hourly variations are deemed minor. Each grid cell in Fig. 4 is colored by the median concentration difference relative to the reference cell. As in Fig. 3 above, cells with no fill color do not meet our data requirements (20 data points over at least nine sampling days). Grey cells correspond to spatial differences smaller than half of all hour-to-hour variations measured by the stationary monitors (Fig. S6). Grey grid cells, therefore, have spatial variations equal to or smaller than typical temporal variations. Red or blue cells indicate absolute spatial differences that are larger than typical hourly variations. Hot colors show that a particular cell has higher concentrations than the reference cell, and cool colors show cells with concentrations smaller than the reference cell. The implication is that the temporal variation measured at a stationary monitor effectively captures the spatial variations in the grey grid cells, but not for red or blue cells.

The approach we use here treats the reference cell as a pseudo-monitor. The exact location of the reference cell does not influence the spatial variation pattern, as we are using the relative concentration difference. Selecting a reference cell with a lower concentration will shift the entire spatial pattern equally.

We do not use the distributed monitor data as the reference for several reasons. Comparing mobile data to mobile data, rather than mobile to stationary, avoids potential issues associated with temporal mismatch (15 min resolution for RAMPs versus 1 Hz or 1 min for mobile), potential confounding factors due to different detection methods for mobile sampling versus RAMPs, and confounding due to different specific sampling locations for mobile and stationary measurements as shown in Fig. 2 for area 8. Additionally, not every distributed monitor is equipped with a CPC, so obtaining UFP spatial differences in every area requires comparing the mobile data to itself.

Both sampling areas shown in Fig. 4 showed spatial heterogeneity of NO_2. The mean absolute NO_2 difference was 2 ppb for both areas, though the maximum NO_2 difference was larger in downtown (area 2, 48 ppb) than in the adjacent residential neighborhood (area 4, 10 ppb). The spatial differences in NO_2 were larger than typical temporal differences; the mean spatial difference of 2 ppb was three times larger than the metric for temporal variation (0.6 ppb, Fig. S6).

UFP was highly dynamic both in space and time. The mean absolute spatial difference in area 2 was 2000 cm^{-3}, and the mean difference in area 4 was 1600 cm^{-3}. The large presence of empty cells in the UFP panels of Fig. 4 was due to data FMPS quality issues as described in Section 2.2. More than half of all colored cells in the UFP maps of Fig. 4 are grey, indicating that the spatial variation was equal to or smaller than our temporal variation metric. This was in part due to the large temporal variability for UFP. The temporal metric for UFP (1800 cm^{-3}) was 30% of regional the background UFP concentration. For NO_2 the temporal metric was only 9% of the regional background.

PM_1 showed inter-cell variability larger than 1 $\mu g\,m^{-3}$ even inside an area of 1 km^2. The mean absolute difference in area 2 was 0.9 $\mu g\,m^{-3}$ and was skewed by a few grid cells with large (4–5 $\mu g\,m^{-3}$) differences from the reference cell. This is likely due to intense local traffic and cooking sources in the central business district (Robinson et al., 2018). PM_1 differences in area 4 were less variable (mean = 0.3 $\mu g\,m^{-3}$, max = 1.3 $\mu g\,m^{-3}$) reflecting fewer sources and the more regional nature of PM. For area 4, the mean spatial difference was half of our temporal metric (0.5 $\mu g\,m^{-3}$) meaning that on average, PM concentrations were not spatially variable in this area.

We can use the information from Fig. 4 to inform the spatial variability in each mobile sampling area. This has implications for siting monitors and evaluating CTMs. Fig. 5 synthesizes the spatial variations across each mobile sampling area. It shows the standard deviation of the differences between each grid cell and the reference cell for NO_2, UFP, and PM_1 in each mobile sampling area. We show the standard deviation, rather than the mean absolute difference because the latter is dependent on the specific choice of the reference cell and the former is not.

We compare pollutant spatial variations to two land use variables in Fig. 5: traffic, represented by vehicle density (vehicle/day/m), and restaurants, represented by restaurant counts. We select these variables because they are related to the sources in our site stratification. The blue lines in Fig. 5 are linear regressions between the standard deviation (SD) of pollutant relative concentration difference from the pseudo monitor and the SD of the land use covariates calculated by dividing each neighborhood into 50 m grid cells.

For both NO_2 and UFP, areas with greater spatial variability in the land use covariates also have greater spatial variability in measured concentrations. Variability in traffic density explains 72% of the variability in NO_2. Both traffic and restaurants are good predictors of UFP variability (traffic R^2 = 0.55, restaurant R^2 = 0.69).

Neither traffic nor restaurants are good predictors for PM_1 spatial variations. This is consistent with the regional nature of PM mass concentrations. PM is more strongly affected by long-range transport and regional secondary PM than local sources (Sampson et al., 2013; Gu et al., 2018).

Fig. 5 essentially shows the error bar for comparing a CTM prediction to measurements in each 1 km^2 area. For many urban areas (2, 3, 4, and 5), the NO_2 spatial variability is 2–4 ppb. Since the regional NO_2 background is 7 ppb, the prediction of a CTM will be "good" if the prediction is within 50% of the actual concentration.

Areas upwind and downwind of the urban core are less spatially variable, and these areas can be reasonably represented by a single stationary monitor. For example, areas 1, 4, 6, and 8 all have PM_1 variations smaller than 1 $\mu g\,m^{-3}$, which is close to the detection limit of nephelometers used in many low-cost distributed sensors, including the RAMP (Malings et al., in prep). Source-impacted areas (2, 3, and 5) have larger PM_1 gradients, indicating that even in an area as small as 1 km^2, a single stationary monitor may not be representative of the entire area.

The downtown area 2 has the highest pollutant concentrations but is not the most spatially variable area in our sampling domain. This area has the highest levels of human activity from traffic and restaurant emissions and the most extreme street canyons but is only slightly

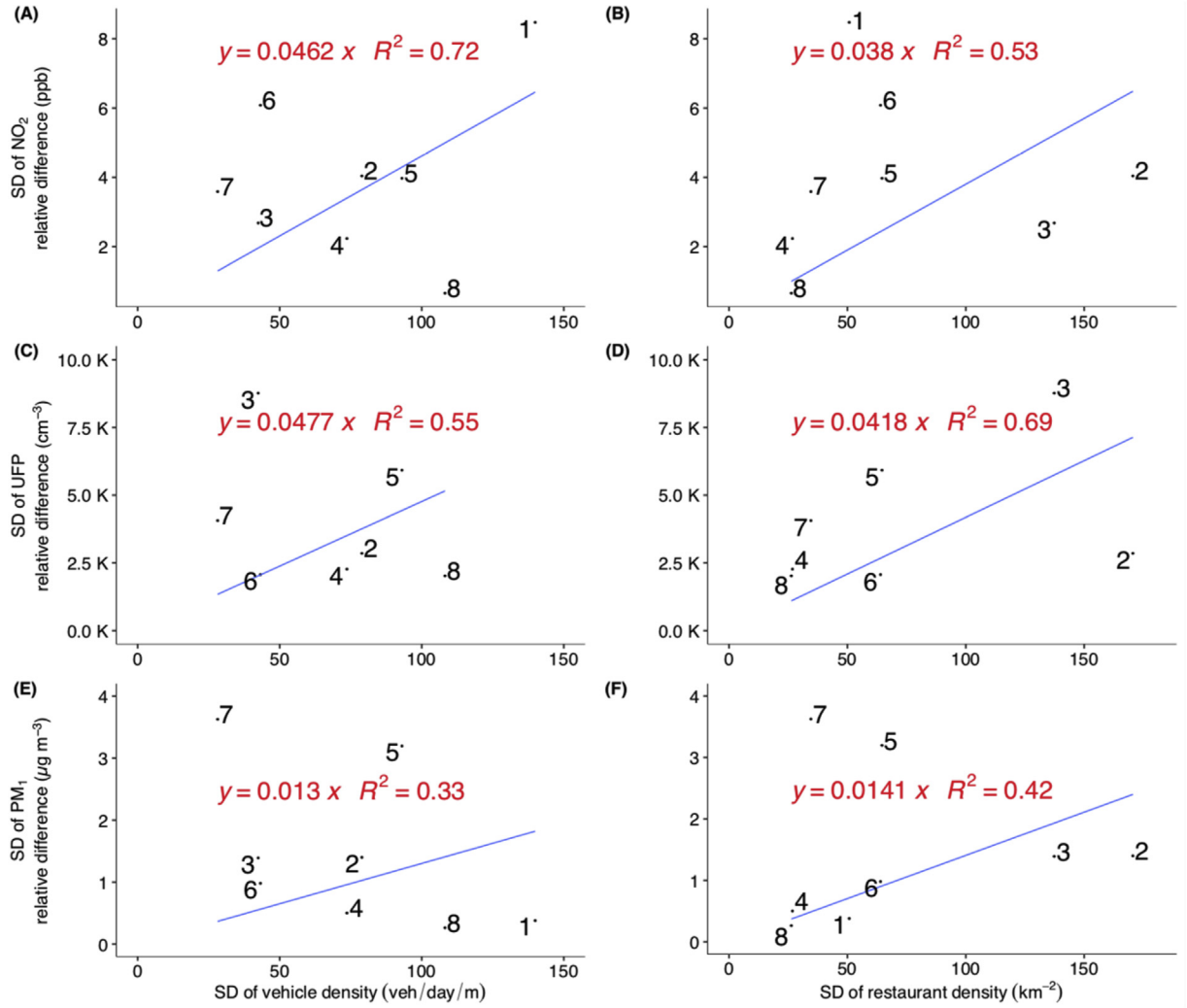

Fig. 5. The standard deviation of concentration difference relative to the reference cell for NO_2 (A–B), UFP (C–D), and PM_1 (E–F) versus standard deviation in land use variables: traffic density (left column) and restaurants density (right column). Linear least-squares regression equations are shown in each panel along with R^2. Site 1 is missing from the UFP panel due to a large fraction of data failing QA/QC checks.

above the median variability across all areas for NO_2, UFP, and PM_1. This suggests that the variability in land use within an area, as shown in Fig. 5, rather than the absolute activity level, is important for determining pollutant spatial variations. Similarly, area 1, which is overall a low-traffic area (Table 1) but has a large variability in traffic, is the most variable area for NO_2.

The data in Fig. 5 can be used to inform how many stationary samplers will be needed to quantify pollutant concentrations within specific tolerances. For example, for NO_2, if the goal of a monitoring network is to constrain all areas within 2 ppb, all areas except area 8 will require more than one sampler per km^2. More variable areas such as 1 and 6 may require more than two stationary monitors per square kilometer to meet this criterion. This can have significant implications for deploying low-cost sensor networks. Deploying more than one sensor per km^2 requires a vast number of sampling locations and is likely unattainable at urban scales (for reference, the City of Pittsburgh is $> 150\,km^2$ and Allegheny County, PA, is $> 1900\,km^2$). A more likely deployment goal will be to quantify pollutant concentrations with less spatial precision or to use a network of samplers to drive a real-time spatial model.

3.4. Statistical evaluation of concentration distributions

Another way to assess spatial variability is to test whether concentrations measured by mobile sampling in each grid cell are statistically different from each other. Fig. 6A shows an example of NO_2 concentrations in downtown Pittsburgh (area 2). We use the Wilcoxon rank-sum test to determine whether each cell is statistically different ($p < 0.05$; blue cells) from the reference cell (black). For this driving area and our choice of the reference cell, approximately 42% of the cells are statistically different from the reference cell, and the remainder are not. Put another way, the reference cell is representative of 58% of this $1\,km^2$ driving area.

Panels 5B-D summarize this analysis for all areas and pollutants. For NO_2, the reference grid cell is representative of 40%–80% of the grid cells in the sampling areas (mean fraction = 62%). We tried relating the fraction of cells similar to the reference to the land use variables like in Fig. 5, but no apparent patterns emerged.

For UFP, the reference cell is representative of 40–90% of the grid cells in each area, similar to NO_2. Source-rich areas like 3 and 4 have lower fractions of cells similar to the reference cell compared with downwind areas (e.g., area 8). This implies that urban monitors represent a smaller surrounding area for human exposures compared to the suburbs. As with NO_2, no apparent relationships were found between the fraction of cells similar to the reference cell and land-use covariates.

PM_1 is more spatially homogeneous than NO_2 or UFP. The reference cell is representative of > 85% of all cells for each mobile sampling

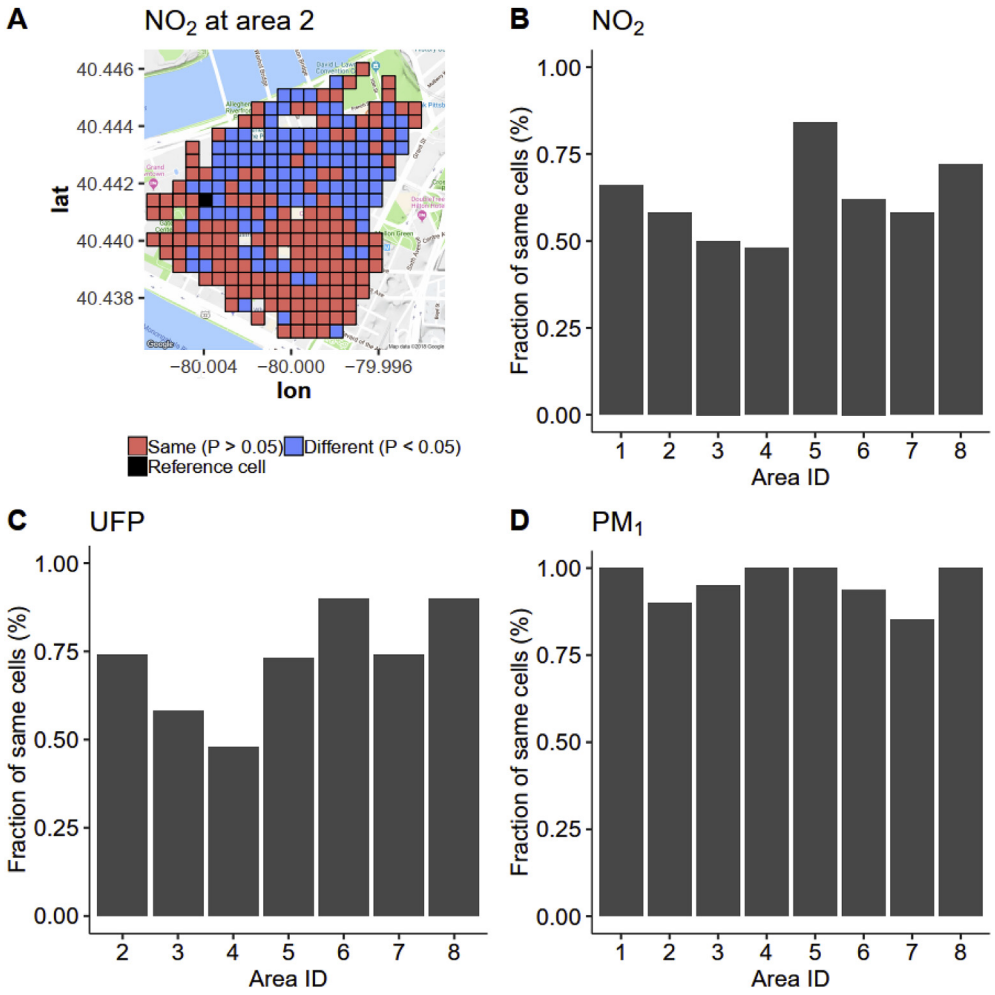

Fig. 6. (A) Distribution of statistically different 50 m cells (Wilcoxon rank-sum test, relative to black reference cell) for NO_2 in downtown area 2. Bar plots show the fraction of statistically nonsignificant cells in each area for NO_2 (B), UFP (C), and PM_1 (D). Site 1 is missing from the UFP panel due to a large fraction of data failing QA/QC checks.

area. For areas 1, 4, 5, and 8, all of the grid cells are statistically similar to the reference cell. This reflects the more regional nature of PM concentrations compared to other pollutants (Robinson et al., 2007; Sampson et al., 2013). Less spatial resolution is needed to determine the underlying PM concentration patterns.

4. Conclusions

Most air pollutants exhibit sub-kilometer scale spatial variations that are not captured by traditional sparse monitoring networks. In this work, we use mobile and distributed monitoring to probe spatial variations in NO_2, UFP, and PM_1 in different urban and background areas.

Our results have implications for quantifying pollutant spatial patterns with low-cost or other distributed monitoring networks. Spatial variations in sub-1 km^2 areas are large enough that a single monitor may not be able to represent even such a small area. For example, for NO_2, most of the neighborhoods have spatial variations that are > 50% of the regional background. For more regional pollutants like PM_1, most of the neighborhoods sampled here have spatial variations that fall within $\sim 1\ \mu g\ m^{-3}$, which is close to the detection limit for many low-cost PM monitors. Quantifying pollutant spatial patterns with high fidelity (e.g., 2 ppb NO_2) seems unattainable in many urban areas unless the sampling network is exceptionally dense, with more than one or two nodes per km^2, in many areas.

In general, locations with more variability in anthropogenic sources such as traffic and restaurants have large pollutant spatial gradients. However, neither traffic nor restaurants can completely describe the observed spatial variability, and other covariates may be necessary for modeling intracity pollutant variation (Eeftens et al., 2012; Li et al., 2018, 2016). Variability in land use seems to be more important as a determining factor for pollutant spatial variations than the absolute activity level. Areas with the highest denity of sources have the highest absolute concentrations but exhibit less sub-km variability than other areas with lower overall activity but higher variability in land use.

The results presented here have implications for the design of future air pollutant monitoring networks. Our results suggest that saturating a city with a sensor network is unlikely to resolve all of the relevant spatial patterns. In the end, high-resolution mapping of cities may require a combination of stationary and mobile monitoring, or high-density monitoring networks will need to be prioritized to focus on specific neighborhoods of concern. There is unlikely to be a single "best" monitoring approach, even in one city. Complete sub-km mapping of a city with sensors or stationary monitors may be unattainable, but saturated sampling of priority areas (e.g., near emissions sources or in environmental justice communities) should be feasible. Future research should focus on the necessary sensor density in specific microenvironments and/or the tradeoffs between stationary pollutant networks and frequent mobile surveys as proposed by Apte et al. (2017).

Data availability

Data are available from the corresponding author on request.

Acknowledgment

This publication was developed under Assistance Agreement No. RD83587301 awarded by the U.S. EPA. It has not been formally reviewed by EPA. The views expressed in this document are solely those of authors and do not necessarily reflect those of the Agency. EPA does not endorse any products or commercial services mentioned in this publication. Funding was also provided by NSF grant number AGS1543786. We thank Jiqiao Shi, Rishabh Shah, and Dr. Aja Ellis for assistance in sampling.

Appendix A. Supplementary data

Supplementary data to this article can be found online at https://doi.org/10.1016/j.aeaoa.2019.100012.

References

Allegheny County Information Portal, 2017. http://infoportal.alleghenycounty.us/data.html (accessed 11.13.2017).

Apte, J.S., Messier, K.P., Gani, S., Brauer, M., Kirchstetter, T.W., Lunden, M.M., Marshall, J.D., Portier, C.J., Vermeulen, R.C.H., Hamburg, S.P., 2017. High-resolution air pollution mapping with google street view cars: exploiting big data. Environ. Sci. Technol. 51, 6999–7008.

Brandt, P.A. van den, 2007. Estimated long-term outdoor air pollution concentrations in a cohort study. Atmos. Environ. 41, 1343–1358.

Brantley, H.L., Hagler, G.S.W., Kimbrough, E.S., Williams, R.W., Mukerjee, S., Neas, L.M., 2014. Mobile air monitoring data-processing strategies and effects on spatial air pollution trends. Atmospheric Meas. Tech. 7, 2169–2183. https://doi.org/10.5194/amt-7-2169-2014.

Brauer, M., Freedman, G., Frostad, J., van Donkelaar, A., Martin, R.V., Dentener, F., Dingenen, R. van, Estep, K., Amini, H., Apte, J.S., Balakrishnan, K., Barregard, L., Broday, D., Feigin, V., Ghosh, S., Hopke, P.K., Knibbs, L.D., Kokubo, Y., Liu, Y., Ma, S., Morawska, L., Sangrador, J.L.T., Shaddick, G., Anderson, H.R., Vos, T., Forouzanfar, M.H., Burnett, R.T., Cohen, A., 2016. Ambient air pollution exposure estimation for the global burden of disease 2013. Environ. Sci. Technol. 50, 79–88. https://doi.org/10.1021/acs.est.5b03709.

Brook, R.D., Rajagopalan, S., Pope, C.A., Brook, J.R., Bhatnagar, A., Diez-Roux, A.V., Holguin, F., Hong, Y., Luepker, R.V., Mittleman, M.A., Peters, A., Siscovick, D., Smith, S.C., Whitsel, L., Kaufman, J.D., 2010. Particulate matter air pollution and cardiovascular disease: an update to the scientific statement from the american heart association. Circulation 121, 2331–2378. https://doi.org/10.1161/CIR.0b013e3181dbece1.

Burnett, R.T., Pope III, C.A.,, Ezzati, M., Olives, C., Lim, S.S., Mehta, S., Shin, H.H., Singh, G., Hubbell, B., Brauer, M., Anderson, H.R., Smith, K.R., Balmes, J.R., Bruce, N.G., Kan, H., Laden, F., Prüss-Ustün, A., Turner, M.C., Gapstur, S.M., Diver, W.R., Cohen, A., 2014. An integrated risk function for estimating the global burden of disease attributable to ambient fine particulate matter exposure. Environ. Health Perspect. https://doi.org/10.1289/ehp.1307049.

City of Pittsburgh GIS Data, 2015. URL http://pghgis-pittsburghpa.opendata.arcgis.com/ (accessed 11.13.2017).

Cohen, A.J., Brauer, M., Burnett, R., Anderson, H.R., Frostad, J., Estep, K., Balakrishnan, K., Brunekreef, B., Dandona, L., Dandona, R., Feigin, V., Freedman, G., Hubbell, B., Jobling, A., Kan, H., Knibbs, L., Liu, Y., Martin, R., Morawska, L., Pope, C.A., Shin, H., Straif, K., Shaddick, G., Thomas, M., van Dingenen, R., van Donkelaar, A., Vos, T., Murray, C.J.L., Forouzanfar, M.H., 2017. Estimates and 25-year trends of the global burden of disease attributable to ambient air pollution: an analysis of data from the Global Burden of Diseases Study 2015. Lancet 389, 1907–1918. https://doi.org/10.1016/S0140-6736(17)30505-6.

Cross, E.S., Williams, L.R., Lewis, D.K., Magoon, G.R., Onasch, T.B., Kaminsky, M.L., Worsnop, D.R., Jayne, J.T., 2017. Use of electrochemical sensors for measurement of air pollution: correcting interference response and validating measurements. Atmos. Meas. Tech. 10, 3575–3588. https://doi.org/10.5194/amt-10-3575-2017.

de Foy, B., 2018. City-level variations in NOx emissions derived from hourly monitoring data in Chicago. Atmos. Environ. 176, 128–139. https://doi.org/10.1016/j.atmosenv.2017.12.028.

de Hoogh, K., Wang, M., Adam, M., Badaloni, C., Beelen, R., Birk, M., Cesaroni, G., Cirach, M., Declercq, C., Dèdelè, A., Dons, E., de Nazelle, A., Eeftens, M., Eriksen, K., Eriksson, C., Fischer, P., Gražulevičienė, R., Gryparis, A., Hoffmann, B., Jerrett, M., Katsouyanni, K., Iakovides, M., Lanki, T., Lindley, S., Madsen, C., Mölter, A., Mosler, G., Nádor, G., Nieuwenhuijsen, M., Pershagen, G., Peters, A., Phuleria, H., Probst-Hensch, N., Raaschou-Nielsen, O., Quass, U., Ranzi, A., Stephanou, E., Sugiri, D., Schwarze, P., Tsai, M.-Y., Yli-Tuomi, T., Varró, M.J., Vienneau, D., Weinmayr, G., Brunekreef, B., Hoek, G., 2013. Development of land use regression models for particle composition in twenty study areas in Europe. Environ. Sci. Technol. 47, 5778–5786. https://doi.org/10.1021/es400156t.

DeCarlo, P.F., Kimmel, J.R., Trimborn, A., Northway, M.J., Jayne, J.T., Aiken, A.C., Gonin, M., Fuhrer, K., Horvath, T., Docherty, K.S., Worsnop, D.R., Jimenez, J.L., 2006. Field-deployable, high-resolution, time-of-flight aerosol mass spectrometer. Anal. Chem. 78, 8281–8289. https://doi.org/10.1021/ac061249n.

Department of City Planning (Pittsburgh), 2017. http://pittsburghpa.gov/dcp (accessed 11.13.2017).

Deshmukh, P., Baldauf, R., Kimbrough, S., Hagler, G., Isakov, V., 2016. Use of high resolution mobile monitoring techniques to assess near-road air quality variability. In: Proceedings of the Air & Waste Management Association Conference.

Di, Q., Dai, L., Wang, Y., Zanobetti, A., Choirat, C., Schwartz, J.D., Dominici, F., 2017a. Association of short-term exposure to air pollution with mortality in older adults. J. Am. Med. Assoc. 318, 2446–2456. https://doi.org/10.1001/jama.2017.17923.

Di, Q., Wang, Yan, Zanobetti, A., Wang, Yun, Koutrakis, P., Choirat, C., Dominici, F., Schwartz, J.D., 2017b. Air pollution and mortality in the medicare population. N. Engl. J. Med. 376, 2513–2522. https://doi.org/10.1056/NEJMoa1702747.

Eeftens, M., Beelen, R., de Hoogh, K., Bellander, T., Cesaroni, G., Cirach, M., Declercq, C., Dèdelè, A., Dons, E., de Nazelle, A., Dimakopoulou, K., Eriksen, K., Falq, G., Fischer, P., Galassi, C., Gražulevičienė, R., Heinrich, J., Hoffmann, B., Jerrett, M., Keidel, D., Korek, M., Lanki, T., Lindley, S., Madsen, C., Mölter, A., Nádor, G., Nieuwenhuijsen, M., Nonnemacher, M., Pedeli, X., Raaschou-Nielsen, O., Patelarou, E., Quass, U., Ranzi, A., Schindler, C., Stempfelet, M., Stephanou, E., Sugiri, D., Tsai, M.-Y., Yli-Tuomi, T., Varró, M.J., Vienneau, D., Klot, S.von, Wolf, K., Brunekreef, B., Hoek, G., 2012. Development of land use regression models for PM2.5, PM2.5 absorbance, PM10 and PMcoarse in 20 European study areas; results of the ESCAPE project. Environ. Sci. Technol. 46, 11195–11205. https://doi.org/10.1021/es301948k.

Friberg, M.D., Kahn, R.A., Holmes, H.A., Chang, H.H., Sarnat, S.E., Tolbert, P.E., Russell, A.G., Mulholland, J.A., 2017. Daily ambient air pollution metrics for five cities: Evaluation of data-fusion-based estimates and uncertainties. Atmos. Environ. 158, 36–50. https://doi.org/10.1016/j.atmosenv.2017.03.022.

Gu, P., Li, H.Z., Ye, Q., Robinson, E.S., Apte, J.S., Robinson, A.L., Presto, A.A., 2018. Intracity variability of particulate matter exposure is driven by carbonaceous sources and correlated with land-use variables. Environ. Sci. Technol. 52, 11545–11554. https://doi.org/10.1021/acs.est.8b03833.

Hama, S.M.L., Cordell, R.L., Kos, G.P.A., Weijers, E.P., Monks, P.S., 2017. Sub-micron particle number size distribution characteristics at two urban locations in Leicester. Atmos. Res. 194, 1–16. https://doi.org/10.1016/j.atmosres.2017.04.021.

Hankey, S., Marshall, J.D., 2015. Land use regression models of on-road particulate air pollution (Particle Number, Black Carbon, PM2.5, Particle Size) using mobile monitoring. Environ. Sci. Technol. 49, 9194–9202.

Harrison, R.M., 2018. Urban atmospheric chemistry: a very special case for study. Npj Clim. Atmospheric Sci. 1, 5. https://doi.org/10.1038/s41612-017-0010-8.

Hatzopoulou, M., Valois, M.F., Levy, I., Mihele, C., Lu, G., Bagg, S., Minet, L., Brook, J., 2017. Robustness of land-use regression models developed from mobile air pollutant measurements. Environ. Sci. Technol. 51, 3938–3947. https://doi.org/10.1021/acs.est.7b00366.

HEI Review Panel on Ultrafine Particles, 2013. Understanding the Health Effects of Ambient Ultrafine Particles, HEI Perspectives 3. Health Effects Institute, Boston, MA.

Jayne, J.T., Leard, D.C., Zhang, X., Davidovits, P., Smith, K.A., Kolb, C.E., Worsnop, D.R., 2000. Development of an aerosol mass spectrometer for size and composition analysis of submicron particles. Aerosol Sci. Technol. 33, 49–70. https://doi.org/10.1080/027868200410840.

Jerrett, M., Burnett, R.T., Ma, R., Pope, C.A., Krewski, D., Newbold, K.B., Thurston, G., Shi, Y., Finkelstein, N., Calle, E.E., Thun, M.J., 2005. Spatial Analysis of Air Pollution and Mortality in Los Angeles. Epidemiology 16, 727–736. https://doi.org/10.1097/01.ede.0000181630.15826.7d.

Jiao, W., Hagler, G., Williams, R., Sharpe, R., Brown, R., Garver, D., Judge, R., Caudill, M., Rickard, J., Davis, M., Weinstock, L., Zimmer-Dauphinee, S., Buckley, K., 2016. Community Air Sensor Network (CAIRSENSE) project: evaluation of low-cost sensor performance in a suburban environment in the southeastern United States. Atmos. Meas. Tech. 9, 5281–5292. https://doi.org/10.5194/amt-9-5281-2016.

Karner, Alex A., Eisinger, D.S., Niemeier, D.A., 2010. Near-Roadway Air Quality: Synthesizing the Findings from Real-World Data. Environ. Sci. Technol. 44, 5334–5344. https://doi.org/10.1021/es100008x.

Kerckhoffs, J., Hoek, G., Messier, K.P., Brunekreef, B., Meliefste, K., Klompmaker, J.O., Vermeulen, R., 2016. Comparison of Ultrafine Particle and Black Carbon Concentration Predictions from a Mobile and Short-Term Stationary Land-Use Regression Model. Environ. Sci. Technol. 50, 12894–12902. https://doi.org/10.1021/acs.est.6b03476.

Kimmel, J.R., Farmer, D.K., Cubison, M.J., Sueper, D., Tanner, C., Nemitz, E., Worsnop, D.R., Gonin, M., Jimenez, J.L., 2011. Real-time aerosol mass spectrometry with millisecond resolution. Int. J. Mass Spectrom. 303, 15–26. https://doi.org/10.1016/j.ijms.2010.12.004.

Klems, J.P., Pennington, M.R., Zordan, C.A., Johnston, M.V., 2010. Ultrafine particles near a roadway intersection: origin and apportionment of fast changes in concentration. Environ. Sci. Technol. 44, 7903–7907. https://doi.org/10.1021/es102009e.

Klompmaker, J.O., Montagne, D.R., Meliefste, K., Hoek, G., Brunekreef, B., 2015. Spatial variation of ultrafine particles and black carbon in two cities: Results from a short-term measurement campaign. Sci. Total Environ. 508, 266–275. https://doi.org/10.1016/j.scitotenv.2014.11.088.

Kumar, P., Morawska, L., Martani, C., Biskos, G., Neophytou, M., Di Sabatino, S., Bell, M., Norford, L., Britter, R., 2015. The rise of low-cost sensing for managing air pollution in cities. Environ. Int. 75, 199–205. https://doi.org/10.1016/j.envint.2014.11.019.

Larson, T., Gould, T., Riley, E.A., Austin, E., Fintzi, J., Sheppard, L., Yost, M., Simpson, C., 2017. Ambient air quality measurements from a continuously moving mobile platform: Estimation of area-wide, fuel-based, mobile source emission factors using absolute principal component scores. Atmos. Environ. 152, 201–211.

Leoni, C., Hovorka, J., Dočekalová, V., Cajthaml, T., Marvanová, S., 2016. Source impact determination using airborne and ground measurements of industrial plumes. Environ. Sci. Technol. 50, 9881–9888. https://doi.org/10.1021/acs.est.6b02304.

Li, H.Z., Dallmann, T.R., Gu, P., Presto, A.A., 2016. Application of mobile sampling to investigate spatial variation in fine particle composition. Atmos. Environ. 142, 71–82. https://doi.org/10.1016/j.atmosenv.2016.07.042.

Li, H.Z., Dallmann, T.R., Li, X., Gu, P., Presto, A.A., 2018. Urban organic aerosol exposure: spatial variations in composition and source impacts. Environ. Sci. Technol. 52, 415–426. https://doi.org/10.1021/acs.est.7b03674.

Lim, S.S., Vos, T., Flaxman, A.D., Danaei, G., Shibuya, K., Adair-Rohani, H., AlMazroa, M.A., Amann, M., Anderson, H.R., Andrews, K.G., Aryee, M., Atkinson, C., Bacchus, L.J., Bahalim, A.N., Balakrishnan, K., Balmes, J., Barker-Collo, S., Baxter, A., Bell, M.L., Blore, J.D., Blyth, F., Bonner, C., Borges, G., Bourne, R., Boussinesq, M., Brauer, M., Brooks, P., Bruce, N.G., Brunekreef, B., Bryan-Hancock, C., Bucello, C., Buchbinder, R., Bull, F., Burnett, R.T., Byers, T.E., Calabria, B., Carapetis, J., Carnahan, E., Chafe, Z., Charlson, F., Chen, H., Chen, J.S., Cheng, A.T.-A., Child, J.C., Cohen, A., Colson, K.E., Cowie, B.C., Darby, S., Darling, S., Davis, A., Degenhardt, L., Dentener, F., Jarlais, D.C.D., Devries, K., Dherani, M., Ding, E.L., Dorsey, E.R., Driscoll, T., Edmond, K., Ali, S.E., Engell, R.E., Erwin, P.J., Fahimi, S., Falder, G., Farzadfar, F., Ferrari, A., Finucane, M.M., Flaxman, S., Fowkes, F.G.R., Freedman, G., Freeman, M.K., Gakidou, E., Ghosh, S., Giovannucci, E., Gmel, G., Graham, K., Grainger, R., Grant, B., Gunnell, D., Gutierrez, H.R., Hall, W., Hoek, H.W., Hogan, A., Hosgood, H.D., Hoy, D., Hu, H., Hubbell, B.J., Hutchings, S.J., Ibeanusi, S.E., Jacklyn, G.L., Jasrasaria, R., Jonas, J.B., Kan, H., Kanis, J.A., Kassebaum, N., Kawakami, N., Khang, Y.-H., Khatibzadeh, S., Khoo, J.-P., Kok, C., Laden, F., Lalloo, R., Lan, Q., Lathlean, T., Leasher, J.L., Leigh, J., Li, Y., Lin, J.K., Lipshultz, S.E., London, S., Lozano, R., Lu, Y., Mak, J., Malekzadeh, R., Mallinger, L., Marcenes, W., March, L., Marks, R., Martin, R., McGale, P., McGrath, J., Mehta, S., Memish, Z.A., Mensah, G.A., Merriman, T.R., Micha, R., Michaud, C., Mishra, V., Hanafiah, K.M., Mokdad, A.A., Morawska, L., Mozaffarian, D., Murphy, T., Naghavi, M., Neal, B., Nelson, P.K., Nolla, J.M., Norman, R., Olives, C., Omer, S.B., Orchard, J., Osborne, R., Ostro, B., Page, A., Pandey, K.D., Parry, C.D., Passmore, E., Patra, J., Pearce, N., Pelizzari, P.M., Petzold, M., Phillips, M.R., Pope, D., Pope, C.A., Powles, J., Rao, M., Razavi, H., Rehfuess, E.A., Rehm, J.T., Ritz, B., Rivara, F.P., Roberts, T., Robinson, C., Rodriguez-Portales, J.A., Romieu, I., Room, R., Rosenfeld, L.C., Roy, A., Rushton, L., Salomon, J.A., Sampson, U., Sanchez-Riera, L., Sanman, E., Sapkota, A., Seedat, S., Shi, P., Shield, K., Shivakoti, R., Singh, G.M., Sleet, D.A., Smith, E., Smith, K.R., Stapelberg, N.J., Steenland, K., Stöckl, H., Stovner, L.J., Straif, K., Straney, L., Thurston, G.D., Tran, J.H., Dingenen, R.V., Donkelaar, A.van, Veerman, J.L., Vijayakumar, L., Weintraub, R., Weissman, M.M., White, R.A., Whiteford, H., Wiersma, S.T., Wilkinson, J.D., Williams, H.C., Williams, W., Wilson, N., Woolf, A.D., Yip, P., Zielinski, J.M., Lopez, A.D., Murray, C.J., Ezzati, M., 2012. A comparative risk assessment of burden of disease and injury attributable to 67 risk factors and risk factor clusters in 21 regions, 1990–2010: a systematic analysis for the Global Burden of Disease Study 2010. Lancet 380, 2224–2260. https://doi.org/10.1016/S0140-6736(12)61766-8.

Carl Malings, Rebecca Tanzer, Aliaksei Hauryliuk, Provat K. Saha, Allen L. Robinson, Albert A. Presto, R Subramanian. Fine Particle Mass Monitoring with Low-Cost Sensors: Corrections and Long-Term Performance Evaluation. Submitted to Aerosol Science & Technology, in prep.

Malings, C., Tanzer, R., Hauryliuk, A., Kumar, S.P.N., Zimmerman, N., Kara, L.B., Presto, A.A., Subramanian, R., 2018. Development of a general calibration model and long-term performance evaluation of low-cost sensors for air pollutant gas monitoring. Atmos. Meas. Tech. Discuss. https://doi.org/10.5194/amt-2018-216.

Marshall, J.D., Apte, J.S., Coggins, J.S., Goodkind, A.L., 2015. Blue Skies Bluer? Environ. Sci. Technol. 49, 13929–13936. https://doi.org/10.1021/acs.est.5b03154.

Messier, K.P., Chambliss, S.E., Gani, S., Alvarez, R., Brauer, M., Choi, J.J., Hamburg, S.P., Kerckhoffs, J., LaFranchi, B., Lunden, M.M., Marshall, J.D., Portier, C.J., Roy, A., Szpiro, A.A., Vermuelen, R.C., Apte, J.S., 2018. Mapping Air Pollution with Google Street View Cars: Efficient Approaches with Mobile Monitoring and Land Use Regression. Environ. Sci. Technol. 52, 12563–12572. https://doi.org/10.1021/acs.est.8b03395.

Petters, M.D., Kreidenweis, S.M., 2007. A single parameter representation of hygroscopic growth and cloud condensation nucleus activity. Atmos. Chem. Phys. 7, 1961–1971. https://doi.org/10.5194/acp-7-1961-2007.

Piersanti, A., Vitali, L., Righini, G., Cremona, G., Ciancarella, L., 2015. Spatial representativeness of air quality monitoring stations: A grid model based approach. Atmospheric Pollut. Res. 6, 953–960. https://doi.org/10.1016/j.apr.2015.04.005.

Pope, C.A.I., Ezzati, M., Dockery, D.W., 2009. Fine-Particulate Air Pollution and Life Expectancy in the United States. N. Engl. J. Med. 360, 376–386.

Raaschou-Nielsen, O., Andersen, Z.J., Beelen, R., Samoli, E., Stafoggia, M., Weinmayr, G., Hoffmann, B., Fischer, P., Nieuwenhuijsen, M.J., Brunekreef, B., Xun, W.W., Katsouyanni, K., Dimakopoulou, K., Sommar, J., Forsberg, B., Modig, L., Oudin, A., Oftedal, B., Schwarze, P.E., Nafstad, P., De Faire, U., Pedersen, N.L., Östenson, C.-G., Fratiglioni, L., Penell, J., Korek, M., Pershagen, G., Eriksen, K.T., Sørensen, M., Tjønneland, A., Ellermann, T., Eeftens, M., Peeters, P.H., Meliefste, K., Wang, M., Bueno-de-Mesquita, B., Key, T.J., de Hoogh, K., Concin, H., Nagel, G., Vilier, A., Grioni, S., Krogh, V., Tsai, M.-Y., Ricceri, F., Sacerdote, C., Galassi, C., Migliore, E., Ranzi, A., Cesaroni, G., Badaloni, C., Forastiere, F., Tamayo, I., Amiano, P., Dorronsoro, M., Trichopoulou, A., Bamia, C., Vineis, P., Hoek, G., 2013. Air pollution and lung cancer incidence in 17 European cohorts: prospective analyses from the European Study of Cohorts for Air Pollution Effects (ESCAPE). Lancet Oncol. 14, 813–822. https://doi.org/10.1016/S1470-2045(13)70279-1.

Robinson, A.L., Donahue, N.M., Shrivastava, M.K., Weitkamp, E.A., Sage, A.M., Grieshop, A.P., Lane, T.E., Pierce, J.R., Pandis, S.N., 2007. Rethinking organic aerosols: semivolatile emissions and photochemical aging. Science 315, 1259–1262. https://doi.org/10.1126/science.1133061.

Robinson, E.S., Gu, P., Zimmerman, N., Ye, Q., Apte, J.S., Robinson, A.L., Presto, A.A., Li, H.Z.S., Rishabh, Apte, J.S., Robinson, A.L., Presto, A.A., Shah, R.U., Apte, J.S., Robinson, A.L., Presto, A.A., 2018. Elevated organic aerosol mass around restaurants with neighborhood-scale influence on air quality. Environ. Sci. Technol. 52, 9285–9294. https://doi.org/10.1021/acs.est.8b02654.

Roohani, Y.H., Roy, A.A., Heo, J., Robinson, A.L., Adams, P.J., 2017. Impact of natural gas development in the Marcellus and Utica shales on regional ozone and fine particulate matter levels. Atmos. Environ. 155, 11–20. https://doi.org/10.1016/j.atmosenv.2017.01.001.

Sabaliauskas, K., Jeong, C.-H., Yao, X., Evans, G.J., 2014. The application of wavelet decomposition to quantify the local and regional sources of ultrafine particles in cities. Atmos. Environ. 95, 249–257. https://doi.org/10.1016/j.atmosenv.2014.05.035.

Saha, P.K., Khlystov, A., Snyder, M.G., Grieshop, A.P., 2018a. Characterization of air pollutant concentrations, fleet emission factors, and dispersion near a North Carolina interstate freeway across two seasons. Atmos. Environ. 177, 143–153. https://doi.org/10.1016/j.atmosenv.2018.01.019.

Saha, P.K., Zimmerman, N., Malings, C., Hauryliuk, A., Li, Z., Snell, L., Subramanian, R., Lipsky, E., Apte, J.S., Robinson, A.L., Presto, A.A., 2019. Quantifying High-resolution Spatial Variations and Local Source Impacts of Urban Ultrafine Particle Concentration. Submitted to. Sci. Tot. Env. 655, 473–481. https://doi.org/10.1016/j.scitotenv.2018.11.197.

Sampson, P.D., Richards, M., Szpiro, A.A., Bergen, S., Sheppard, L., Larson, T.V., Kaufman, J.D., 2013. A regionalized national universal kriging model using Partial Least Squares regression for estimating annual PM2.5 concentrations in epidemiology. Atmos. Environ. 75, 383–392. https://doi.org/10.1016/j.atmosenv.2013.04.015.

Shi, Y., Lau, K.K.-L., Ng, E., 2016. Developing street-level PM2.5 and PM10 land use regression models in high-density Hong Kong with urban morphological factors. Environ. Sci. Technol. 50, 8178–8187. https://doi.org/10.1021/acs.est.6b01807.

Simon, M.C., Hudda, N., Naumova, E.N., Levy, J.I., Brugge, D., Durant, J.L., 2017. Comparisons of traffic-related ultrafine particle number concentrations measured in two urban areas by central, residential, and mobile monitoring. Atmos. Environ. 169, 113–127. https://doi.org/10.1016/j.atmosenv.2017.09.003.

Snyder, E.G., Watkins, T.H., Solomon, P.A., Thoma, E.D., Williams, R.W., Hagler, G.S.W., Shelow, D., Hindin, D.A., Kilaru, V.J., Preuss, P.W., 2013. The changing paradigm of air pollution monitoring. Environ. Sci. Technol. 47, 11369–11377. https://doi.org/10.1021/es4022602.

Spinelle, L., Gerboles, M., Villani, M.G., Aleixandre, M., Bonavitacola, F., 2015. Field calibration of a cluster of low-cost available sensors for air quality monitoring. Part A: Ozone and nitrogen dioxide. Sensor. Actuator. B Chem. 215, 249–257. https://doi.org/10.1016/j.snb.2015.03.031.

Stafoggia, M., Schneider, A., Cyrys, J., Samoli, E., Andersen, Z.J., Bedada, G.B., Bellander, T., Cattani, G., Eleftheriadis, K., Faustini, A., Hoffmann, B., Jacquemin, B., Katsouyanni, K., Massling, A., Pekkanen, J., Perez, N., Peters, A., Quass, U., Yli-Tuomi, T., Forastiere, F., Group, on behalf of the U.S., 2017. Association between short-term exposure to ultrafine particles and mortality in eight European Urban areas. Epidemiology 28, 172–180. https://doi.org/10.1097/EDE.0000000000000599.

Steffens, J., Kimbrough, S., Baldauf, R., Isakov, V., Brown, R., Powell, A., Deshmukh, P., 2017. Near-port air quality assessment utilizing a mobile measurement approach. Atmos. Pollut. Res. 8 (6), 1023–1030.

Strak, M., Janssen, N., Beelen, R., Schmitz, O., Vaartjes, I., Karssenberg, D., van den Brink, C., Bots, M.L., Dijst, M., Brunekreef, B., Hoek, G., 2017. Long-term exposure to particulate matter, NO2 and the oxidative potential of particulates and diabetes prevalence in a large national health survey. Environ. Int. 108, 228–236. https://doi.org/10.1016/j.envint.2017.08.017.

Tan, Y., Lipsky, E.M., Saleh, R., Robinson, A.L., Presto, A.A., 2014a. Characterizing the spatial variation of air pollutants and the contributions of high emitting vehicles in Pittsburgh, PA. Environ. Sci. Technol. 48, 14186–14194. https://doi.org/10.1021/es5034074.

Tan, Y., Robinson, A.L., Presto, A.A., 2014b. Quantifying uncertainties in pollutant mapping studies using the Monte Carlo method. Atmos. Environ. 99, 333–340. https://doi.org/10.1016/j.atmosenv.2014.10.003.

Tan, Y., Dallmann, T.R., Robinson, A.L., Presto, A.A., 2016. Application of plume analysis to build land use regression models from mobile sampling to improve model transferability. Atmos. Environ. 134, 51–60. https://doi.org/10.1016/j.atmosenv.2016.03.032.

Tang, R., Blangiardo, M., Gulliver, J., 2013. Using building heights and street configuration to enhance intraurban PM10, NOx, and NO2 land use regression models. Environ. Sci. Technol. 47, 11643–11650. https://doi.org/dx.doi.org/10.1021/es402156g.

U.S. Census TIGER, 2010. https://www.census.gov/geo/maps-data/data/tiger.html (accessed 11.13.2017).

Van den Bossche, J., Theunis, J., Elen, B., Peters, J., Botteldooren, D., De Baets, B., 2016. Opportunistic mobile air pollution monitoring: A case study with city wardens in Antwerp. Atmos. Environ. 141, 408–421.

Vardoulakis, S., Gonzalez-Flesca, N., Fisher, B.E.A., Pericleous, K., 2005. Spatial variability of air pollution in the vicinity of a permanent monitoring station in central Paris. Atmos. Environ. 39, 2725–2736. https://doi.org/10.1016/j.atmosenv.2004.05.067.

Vert, C., Meliefste, K., Hoek, G., 2016. Outdoor ultrafine particle concentrations in front of fast food restaurants. J. Expo. Sci. Environ. Epidemiol. 26, 35–41. https://doi.org/10.1038/jes.2015.64.

Vitali, L., Morabito, A., Adani, M., Assennato, G., Ciancarella, L., Cremona, G., Giua, R., Pastore, T., Piersanti, A., Righini, G., Russo, F., Spagnolo, S., Tanzarella, A., Tinarelli, G., Zanini, G., 2016. A Lagrangian modelling approach to assess the representativeness area of an industrial air quality monitoring station. Atmospheric Pollut. Res. 7,

990–1003. https://doi.org/10.1016/j.apr.2016.06.002.
Wang, M., Beelen, R., Basagana, X., Becker, T., Cesaroni, G., de Hoogh, K., Dedele, A., Declercq, C., Dimakopoulou, K., Eeftens, M., Forastiere, F., Galassi, C., Gražulevičienė, R., Hoffmann, B., Heinrich, J., Iakovides, M., Künzli, N., Korek, M., Lindley, S., Mölter, A., Mosler, G., Madsen, C., Nieuwenhuijsen, M., Phuleria, H., Pedeli, X., Raaschou-Nielsen, O., Ranzi, A., Stephanou, E., Sugiri, D., Stempfelet, M., Tsai, M.-Y., Lanki, T., Udvardy, O., Varró, M.J., Wolf, K., Weinmayr, G., Yli-Tuomi, T., Hoek, G., Brunekreef, B., 2013. Evaluation of land use regression models for NO2 and particulate matter in 20 European study areas: the ESCAPE project. Environ. Sci. Technol. 47, 4357–4364. https://doi.org/10.1021/es305129t.
Ye, Q., Gu, P., Li, H.Z., Robinson, E.S., Lipsky, E., Kaltsonoudis, C., Lee, A.K.Y., Apte, J.S., Robinson, A.L., Sullivan, R.C., Presto, A.A., Donahue, N.M., 2018. Spatial variability of sources and mixing state of atmospheric particles in a metropolitan area. Environ. Sci. Technol. 52, 6807–6815. https://doi.org/10.1021/acs.est.8b01011.
Zimmerman, N., Jeong, C.-H., Wang, J.M., Ramos, M., Wallace, J.S., Evans, G.J., 2015. A source-independent empirical correction procedure for the fast mobility and engine exhaust particle sizers. Atmos. Environ. 100, 178–184. https://doi.org/10.1016/j.atmosenv.2014.10.054.
Zimmerman, N., Presto, A.A., Kumar, S.P.N., Gu, J., Hauryliuk, A., Robinson, E.S., Robinson, A.L., Subramanian, R., 2018a. A machine learning calibration model using random forests to improve sensor performance for lower-cost air quality monitoring. Atmos. Meas. Tech. 11, 291–313. https://doi.org/10.5194/amt-11-291-2018.
Zimmerman, N., Robinson, E.S., Li, H.Z., Ellis, A., Subramanian, R., Robinson, A.L., Apte, J.S., Presto, A.A., 2018b. Integrating spatiotemporal variability and modifiable factors into air pollution estimates: the center for air, climate, and energy solutions air quality observatory. Submitted to. Atmospheric Environment Manuscript number ATMENV-D-18-01018.